Localized outbreaks in S-I-R model with diffusion

Chunyi Gai, David Iron and Theodore Kolokolnikov

Department of Mathematics and Statistics, Dalhousie University, Halifax, Canada

We investigate an SIRS epidemic model with spatial diffusion and nonlinear incidence rates. We show that for small diffusion rate of the infected class D_I, the infected population tends do be highly localized at certain points inside the domain, forming K spikes. We then study three distinct destabilization mechanisms, as well as a transition from localized spikes to plateau solutions. Two of the instabilities are due to coarsening (spike death) and self-replication (spike birth), and have well-known analogues in other reaction-diffusion systems such as the Schnakenberg model. The third transition is when a single spike becomes unstable and moves to the boundary. This happens when the diffusion of the recovered class, D_R becomes sufficiently small. In all cases, the stability thresholds are computed asymptotically and are verified by numerical experiments. We also show that the spike solution can transit into an plateau-type solution when the diffusion rates of recovered and susceptible class are sufficiently small. Implications for disease spread and control through quarantine are discussed.

1. INTRODUCTION

The SIRS epidemic model introduced by Kermack and McKendrick in 1927 [1] is widely used to model the spread of infectious diseases. The population is divided into three disjoint classes: susceptible (S), infected (I), and recovered (R), where susceptibles can be infected by those already infected and subsequently recover, and recovered class are immune to the disease but lose immunity over time. These assumptions are modelled using the following system of ODEs:

$$\begin{cases} S_t = -\beta SI + \gamma R, \\ I_t = \beta SI - \nu I, \\ R_t = \nu I - \gamma R, \end{cases} \tag{1}$$

where β is the infection rate, ν is the recovery rate, and γ is the rate of immunity loss. Kermack and McKendrick's work has motivated the use of mathematics in the study of epidemiology [2–4].

While spatially-homogeneous dynamics are by now well studied, modelling spatial interactions is still an active area of research. Most disease outbreaks have a strong spatial characterisitic, and many studies emphasize the importance of the spatial dimension for modelling these outbreaks. For example, [5] looked at spatio-temporal patterns in HIV outbreaks in Malawi over two decades (1994-2010). The authors found that the disease initially spread in several localized hot-spots and they identified several geographically differentiated HIV/AIDS epidemics rather than a single one. These initial outbreaks were followed by a complex spatio-temporal dynamics. Similar spatial clusters of HIV outbreaks were found in a recent study [6] in Phayao Province, Thailand, and in South Africa [7].

In recent decades, numerous methodologies have been used to describe spatial distribution of diesease. This include the use of cellular automata [8, 9], metapopulations [10–12], networks [13, 14] and partial differential equations [15, 16]. Generally speaking, incorporating spatial structure leads to very rich dynamics in epidemic models, such as formation of disease hot-spots.

In this paper we study spatially-localized outbreaks for the SIRS model with spatial dispersion. As will be shown below, such outbreaks can occur when the infection rate β is nonlinear. For simplicity, we will assume that β is proportional to I, although other types of nonlinearity, such as Holling functional response also lead to hot-spot formation. We model spatial dispersion using diffusion. This results in the following system,

$$\begin{cases} S_t = D_S S_{xx} - \chi SI^2 + \gamma R, \\ I_t = D_I I_{xx} + \chi SI^2 - \nu I, \\ R_t = D_R R_{xx} + \nu I - \gamma R. \end{cases} \tag{2}$$

Here D_S, D_I, D_R are diffusion coefficients of each class of population, χI is the rate of infection. We study the epidemic system on 1-D interval $[-L, L]$ with Neumann boundary conditions, so that $S_x = I_x = R_x = 0$ at $x = \pm L$. For simplicity, we also assume the timescale of infection and recovery is much shorter than the average life span, so birth and death rates for each class are neglected.

The second key assumption we make is that the infected class I diffuses more slowly than others. There are two scenarios where this is biologically plausible. The first scenario, common in many species is that the disease itself reduces the species mobility. A second scenario, applicable to humans, is an intentional quarantene policy to limit the spread of infection. Such a policy is well known to be effective in controlling disease outbreaks and is often used a first-line defense against quickly-spreading infections.

We therefore write $D_I = \varepsilon^2$ where ε is small. By further rescaling [17], we may set $\chi = 1, \nu = 1$. This leads to the following singularly perturbed reaction diffusion system:

$$\begin{cases} S_t = D_S S_{xx} - SI^2 + \gamma R, \\ I_t = \varepsilon^2 I_{xx} + SI^2 - I, \\ R_t = D_R R_{xx} + I - \gamma R. \end{cases} \tag{3}$$

Under these assumptions, this system has localized disease concentrations corresponding to spike-type solutions. Such spike patterns have been studied in great detail since 1990's in simpler reaction-diffusion systems consisting of two components, such as Gierer-Meinhardt system, Gray-Scott model, Schnakenberg model and Keller-Segel model and its variants. We refer reader to [18–30] and references therein. The introduction of a third component leads to interesting new phenomena not present in two-component reaction-diffusion systems [31].

Let us summarize the main results in this paper. Simulations and analysis show that the behavior of the system is highly dependent on diffusion rate D_R, relative to the diffusion rate of infected class, ε^2. We isolate two distinct regimes: either $D_R \gg O(\varepsilon^2)$ or $D_R \leq O(\varepsilon^2)$.

The regime $D_R \gg O(\varepsilon^2)$ is studied in Sections 2, 3, 5. In this regime, the steady-state population consists of K hot-spots of disease, uniformly distributed inside the interval $[-L, L]$. Depending on system parameters, the K-spike steady state can undergo two types of instabilities. The first type, analyzed in Section 5 5.1 is referred to as *spike competition instability*. As a result of such an instability, some of the hot-spots are "absorbed" by others, resulting in fewer hot-spots. The second type of instability, studied in 5 5.2 is referred to as *self-replication instability*, whereby a spike splits into two, resulting in more spikes. These instabilities are illustrated in Figure 1. Figure 1(a) shows 8 spikes that gradually coarsen into 2 as D_S is gradually increased. On the other hand, with one-spike equilibrium as initial condition, replication occurs and more spikes appear as we gradually decrease D_S. This is shown in Fig 1(b). We derive explicit thresholds for D_S such that the spike competition occurs when $D_S > D_{SK}^{com}$, $K \geq 2$; and self-replication instability occurs when $D_S < D_{SK}^{rep}$, $K \geq 1$. Formulas for D_{SK}^{com} and D_{SK}^{rep} are given in Section 5.

The second regime we study is when D_R is small: $D_R \leq O(\varepsilon^2)$. In this case, a single spike can become unstable, and depending on other parameters, two phenomena can occur. If D_R is sufficiently small, a single spike moves to the boundary (depending on how big D_S is), as illustrated in Figure 2. This phenomenon is studied in Section 4. On the other hand, when both D_R and D_S are small, the spike "fattens up" and becomes a mesa-type pattern, i.e. a contiguous region of high concentration of disease connected via a sharp interface to a region of low concentration. Numerically we observe two types of inhomogeneous equilibrium depending on the value of D_S and an example of such a steady state pattern is shown in Figure 3. Spike-type solution exists for sufficiently large D_S, but transition to interface-type patterns for small D_S. This process is illustrated in Figure 3(left). Interface patterns are studied in Section 6.

(a)　　　　　　　　　　　　　　(b)
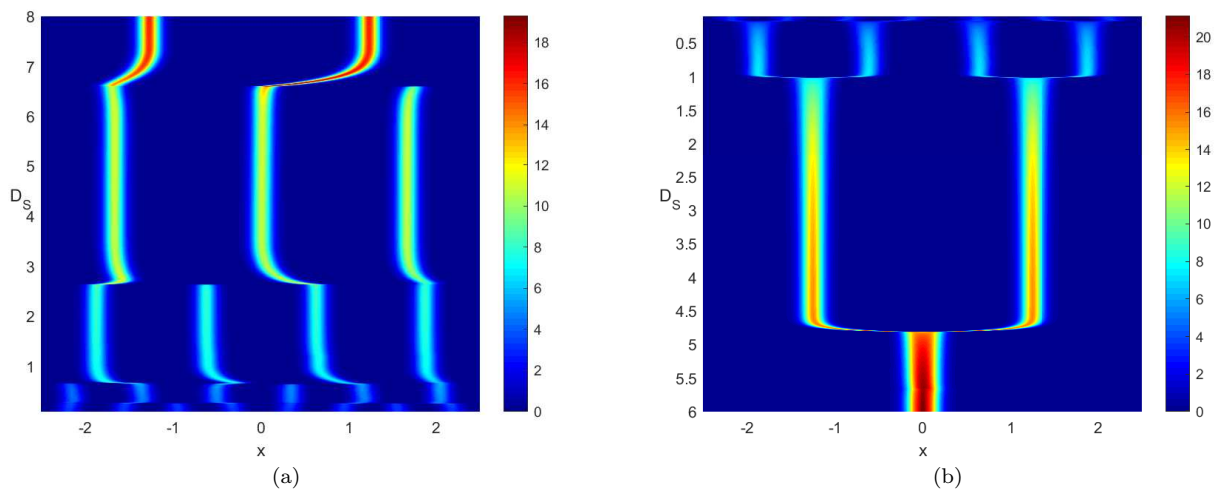
FIG. 1. Instabilities of steady state spike solutions induced by slowly increasing D_S or decreasing D_S. Here $D_R = 1, L = 2.5, \varepsilon = 0.05, N = 15$ and $\gamma = 1$. Left: Coarsening (competition) instability when D_S is increased ($D_s = 1 + 10^{-5}t$). Colour plot of I is shown. Right: Self-replication instability when D_S is slowly decreased ($D_s = 6 - 10^{-5}t$).

(a) $D_R = 1$

(b) $D_R = 0.0036$
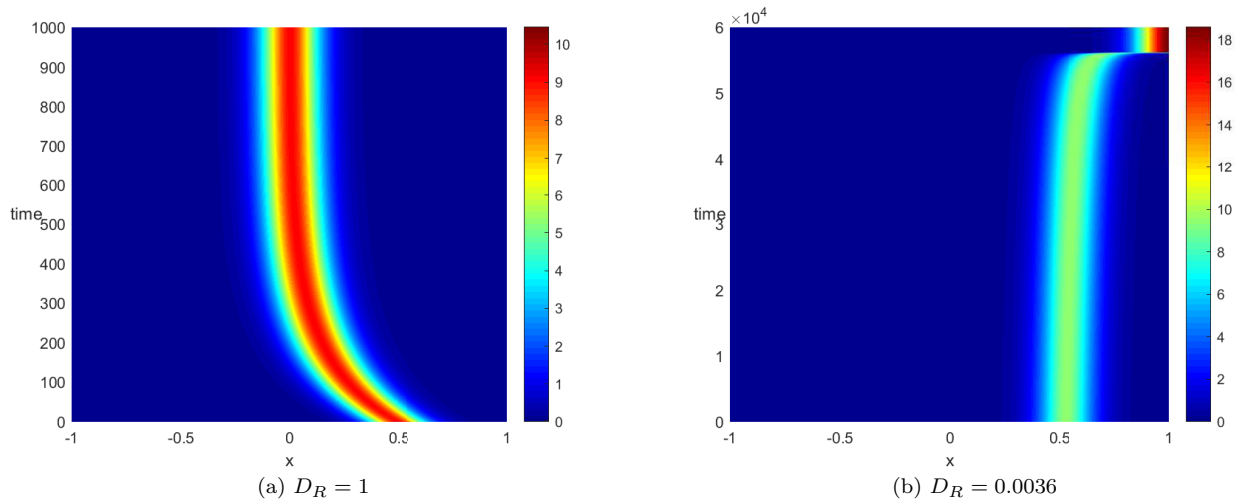
FIG. 2. Stable and unstable motion of a single spike. Here, D_R is as indicated while other parameters are fixed at $D_S = 5, L = 1, \varepsilon = 0.06, N = 5$ and $\gamma = 1$. In (a), one-spike equilibrium moves to the center, which shows that the center spike is stable. In (b) the spike moves to boundary instead of moving to center, so that a single spike is unstable.

$D_S = 1$

$D_S = 0.05.$
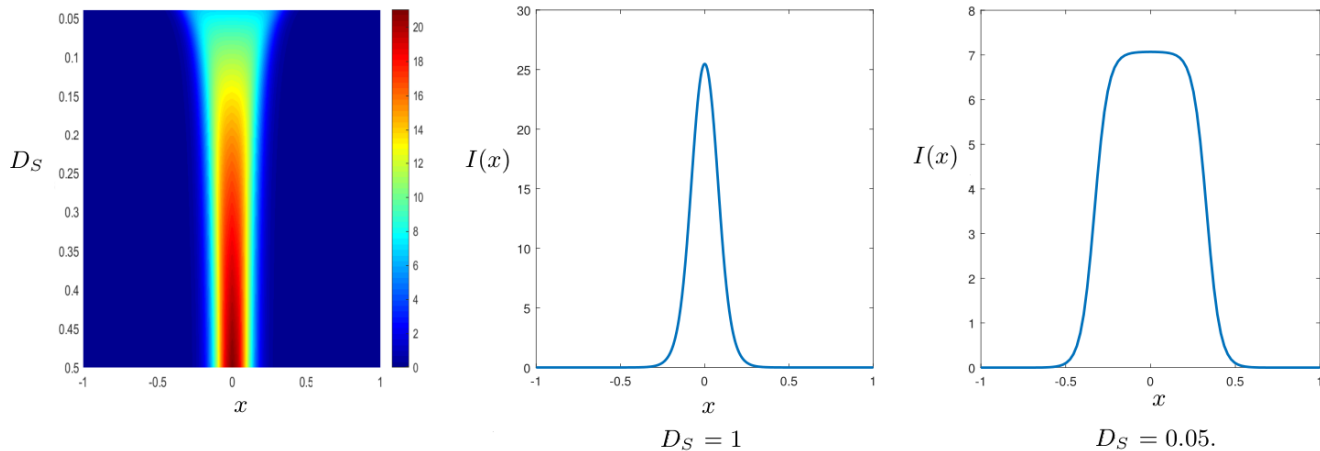
FIG. 3. Transition from spike to mesa when $D_R = 0, \varepsilon = 0.04, N = 10, L = 1, \gamma = 1$ with D_S as a control parameter. Left: D_S is gradually decreased from 0.5 to 0.05. Middle, Right: Profile of $I(x)$ for D_S as indicated.

2. SINGLE-SPIKE SOLUTION

We start by constructing a single interior spike solution to (3). Such a solution corresponds to a localized concentration of the infected population I at some point x_0 in the interior of the domain, $x_0 \in (-L, L)$. The extent of the spike is of $O(\varepsilon)$. We therefore introduce the inner variable

$$y = \frac{x - x_0}{\varepsilon}. \tag{4}$$

In the inner region, equilibrium solution of (3) then becomes

$$\begin{cases} S_{yy} - \frac{\varepsilon^2}{D_S} S I^2 + \frac{\varepsilon^2}{D_S} \gamma R = 0, \\ I_{yy} + S I^2 - I = 0, \\ R_{yy} + \frac{\varepsilon^2}{D_R} I - \frac{\varepsilon^2}{D_R} \gamma R = 0. \end{cases} \tag{5}$$

We then expand S, I, R as

$$
\begin{aligned}
S &= S_0 + \varepsilon S_1 + O(\varepsilon^2), \\
I &= I_0 + \varepsilon I_1 + O(\varepsilon^2), \\
R &= R_0 + \varepsilon R_1 + O(\varepsilon^2).
\end{aligned}
\tag{6}
$$

Upon substituting (6) into (5) and collecting higher-order terms in ε, we obtain, to leading order,

$$
\begin{cases}
S_{0yy} = 0, \\
I_{0yy} + S_0 I_0^2 - I_0 = 0, \\
R_{0yy} = 0.
\end{cases}
\tag{7}
$$

This shows that S_0 and R_0 are constants to be determined. We then rescale

$$
I_0 = \frac{1}{S_0} w(y),
\tag{8}
$$

where so that w satisfies the well-known ground-state

$$
w'' - w + w^2 = 0, \quad w \to 0 \text{ as } y \to \pm\infty
$$

whose explicit solution is given by

$$
w(y) = \frac{3}{2}\text{sech}^2\left(\frac{y}{2}\right).
$$

To determine R_0 and S_0, we must match the inner and the outer region. In the outer region we approximate $I \sim \left(\int_{-L}^{L} I\, dx\right)\delta(x - x_0)$ and $SI^2 \sim \left(\int_{-L}^{L} SI^2 dx\right)\delta(x - x_0)$. We further estimate $\left(\int_{-L}^{L} I\, dx\right) \sim \frac{1}{S_0}\varepsilon\int_{-\infty}^{\infty} w\, dy \sim 6\varepsilon/S_0$ and similarly, $\int_{-L}^{L} SI^2 dx \sim 6\varepsilon/S_0$, so that

$$
\begin{aligned}
0 &= D_S S_{xx} + \gamma R - 6\varepsilon/S_0 \delta(x - x_0), \\
0 &= D_R R_{xx} - \gamma R + 6\varepsilon/S_0 \delta(x - x_0).
\end{aligned}
\tag{9}
$$

To solve (9), we introduce the modified Green's function $G(x; x_0)$, which satisfies

$$
\begin{cases}
G_{xx} - \frac{\gamma}{D_R} G = -\delta(x; x_0), \\
G_x(x_0^+) - G_x(x_0^-) = -1, \\
G_x(\pm L) = 0.
\end{cases}
\tag{10}
$$

A simple calculation gives

$$
G(x; x_0) =
\begin{cases}
\dfrac{\cosh\left(\sqrt{\frac{\gamma}{D_R}}(x+L)\right)\cosh\left(\sqrt{\frac{\gamma}{D_R}}(x_0-L)\right)}{\sqrt{\frac{\gamma}{D_R}}\sinh(2\sqrt{\frac{\gamma}{D_R}}L)}, & -L < x < x_0 \\[4mm]
\dfrac{\cosh\left(\sqrt{\frac{\gamma}{D_R}}(x_0+L)\right)\cosh\left(\sqrt{\frac{\gamma}{D_R}}(x-L)\right)}{\sqrt{\frac{\gamma}{D_R}}\sinh(2\sqrt{\frac{\gamma}{D_R}}L)}, & x_0 < x < L.
\end{cases}
\tag{11}
$$

The solution to (9) is then given by

$$
R(x) = \frac{6\varepsilon}{S_0 D_R} G(x; x_0)
\tag{12}
$$

and

$$
S(x) = -\frac{D_R}{D_S} R(x) + \frac{D_R}{D_S} R_0 + S_0,
\tag{13}
$$

where $R_0 = \frac{6\varepsilon}{S_0 D_R} G(x; x_0)$ and S_0 is to be determined.

To find S_0, we use the conservation of mass. Let N be the total population, so that

$$
N \equiv \int_{-L}^{L} S + I + R\, dx.
\tag{14}
$$

Note that by adding three equations in (3) and integrating over the domain, N is independent of time. We will also take

$$N = 2N_0 L, \tag{15}$$

where N_0 is an arbitrary constant depending on initial conditions, so that N scales with domain size; N_0 can be thought of an average density.

We now substitute (8), (12) and (13) into the mass conservation condition (14, 15) to obtain that

$$S_0^2 - N_0 S_0 + E = 0, \tag{16}$$

where

$$E = \frac{3\varepsilon}{L}\left(1 + \frac{1}{\gamma} - \frac{D_R}{\gamma D_S} + 2\sqrt{\frac{D_R}{\gamma}}\frac{L}{D_S}\frac{\cosh(\sqrt{\frac{\gamma}{D_R}}(x_0+L))\cosh(\sqrt{\frac{\gamma}{D_R}}(x_0-L))}{\sinh(2\sqrt{\frac{\gamma}{D_R}}L)}\right). \tag{17a}$$

Solving (16) we get two roots when $N_0^2 - 4E > 0$. Asymptotically in ε, they are

$$S_{0-} \sim \frac{E}{N_0}, \tag{17b}$$

which is of $O(\varepsilon)$ and

$$S_{0+} \sim N_0, \tag{17c}$$

which is of $O(1)$. Plots of these two roots are shown in Fig 4. The two roots connect at a fold point corresponding to a double root of (16).

We now summarize our first result:
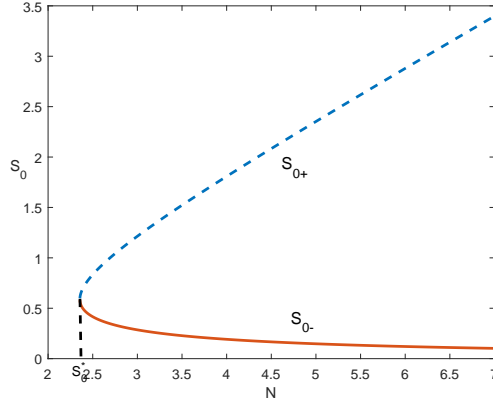
FIG. 4. Plot of two roots to (16) vs. total population N. Here $\varepsilon = 0.05, L = 1, D_R = 1, D_S = 1$ and $\gamma = 1$. The dashed curve denotes S_{0+} and the solid curve denotes S_{0-}. S_0^* is the fold point where (16) has double root.

Result 2.1 *With $D_I = \varepsilon^2$ and $0 < \varepsilon \ll 1$, the SIRS system (3) has the following single-spike steady state:*

$$S(x) \sim -\frac{6\varepsilon}{S_0 D_S}G(x;x_0) + \frac{6\varepsilon}{S_0 D_S}G(x_0;x_0) + S_0,$$

$$I(x) \sim \frac{1}{S_0}w\left(\frac{x-x_0}{\varepsilon}\right), \tag{18}$$

$$R(x) \sim \frac{6\varepsilon}{S_0 D_R}G(x;x_0),$$

where $G(x;x_0)$ is given by (11), $w(y) = \frac{3}{2}\operatorname{sech}^2(\frac{y}{2})$ and S_0 is a constant determined by the total population mass as given in (17).

3. NONLOCAL EIGENVALUE PROBLEM

We now study the stability of one-spike solution. We first linearize around the steady state by taking

$$
S(x,t) = S(x) + e^{\lambda t}\varphi(x),
$$
$$
I(x,t) = I(x) + e^{\lambda t}\psi(x),
$$
$$
R(x,t) = R(x) + e^{\lambda t}\xi(x).
$$

Assuming $|\varphi|, |\psi|, |\xi| \ll O(1)$ we obtain the linearized problem

$$
\begin{cases}
\lambda\varphi = D_S\varphi_{xx} - I_0^2\varphi - 2S_0 I_0\psi + \gamma\xi, \\
\lambda\psi = \varepsilon^2\psi_{xx} + I_0^2\varphi + (2S_0 I_0 - 1)\psi, \\
\lambda\xi = D_R\xi_{xx} + \psi - \gamma\xi.
\end{cases}
\tag{19}
$$

In the inner region, we let $y = \frac{x-x_0}{\varepsilon}$ where x_0 is the spike position. To leading order, we then obtain $\varphi_{yy} \sim 0$ so that $\varphi(x) \sim \varphi_0$ is constant to be determined. The equation for ψ is

$$
\lambda\psi = \psi_{yy} - \psi + 2w(y)\psi + I_0^2\varphi_0.
\tag{20}
$$

In the outer region, we approximate

$$
\begin{cases}
D_S\varphi_{xx} - \lambda\varphi + \gamma\xi = c_1\delta(x;x_0), \\
D_R\xi_{xx} - (\gamma + \lambda)\xi = c_2\delta(x;x_0).
\end{cases}
\tag{21}
$$

where

$$
c_1 = \left(\varphi_0\int I_0^2 dx + 2S_0\int I_0\psi dx\right), \quad c_2 = -\int\psi dx.
\tag{22}
$$

We write

$$
\xi(x;x_0) = -\frac{c_2}{D_R}G\left(x;x_0,\sqrt{\frac{\gamma+\lambda}{D_R}}\right),
\tag{23}
$$

where $G(x;x_0,\mu)$ is the Green's function that satisfies

$$
\begin{cases}
G_{xx} - \mu^2 G = -\delta(x;x_0), \\
G_x(\pm L) = 0,
\end{cases}
\tag{24}
$$

and is explicitly given by

$$
G = \frac{1}{\mu\sinh(2\mu L)}\begin{cases}
\cosh\left(\mu(x+L)\right)\cosh\left(\mu(x_0-L)\right), & -L < x < x_0 \\
\cosh\left(\mu(x_0+L)\right)\cosh\left(\mu(x-L)\right), & x_0 < x < L.
\end{cases}
\tag{25}
$$

To solve for φ, we make a change of variables. Let

$$
\varphi = \frac{D_R\gamma}{\lambda(D_R - D_S) - \gamma D_S}\xi + \varphi_h.
\tag{26}
$$

Then φ_h satisfies:

$$
D_S\varphi_{hxx} - \lambda\varphi_h = \left(c_1 - \frac{\gamma c_2}{\lambda(D_R - D_S) - \gamma D_S}\right)\delta(x;x_0)
$$

so that

$$
\varphi_h = -\frac{1}{D_S}\left(c_1 - \frac{\gamma c_2}{\lambda(D_R - D_S) - \gamma D_S}\right)G\left(x;x_0;\sqrt{\frac{\lambda}{D_s}}\right)
$$

Therefore we estimate

$$
\varphi_0 = \varphi(x_0) \sim -c_2\frac{\gamma}{\lambda(D_R - D_S) - \gamma D_S}G\left(x_0;x_0,\sqrt{\frac{\gamma+\lambda}{D_R}}\right) - \frac{1}{D_S}\left(c_1 - \frac{\gamma c_2}{\lambda(D_R - D_S) - \gamma D_S}\right)G\left(x_0;x_0;\sqrt{\frac{\lambda}{D_s}}\right)
$$

and

$$c_1 = \varepsilon \left(\frac{\varphi_0}{S_0^2} \int w^2 dy + 2 \int w\psi dy \right); \quad c_2 = -\varepsilon \int \psi dy. \tag{27}$$

After some algebra, this leads to the following non-local eigenvalue problem (NLEP),

$$(L_0 - \lambda)\psi = w^2 \frac{2}{\int_{-\infty}^{\infty} w^2 dy - (\lambda+1)\frac{S_0^2}{\varepsilon P}} \int_{-\infty}^{\infty} w\psi dy, \tag{28}$$

$$\text{where } L_0\psi = \psi_{yy} - \psi + 2w\psi \tag{29}$$

and where

$$P = \frac{\gamma\sqrt{\frac{D_R}{\lambda+\gamma}}}{\lambda(D_R - D_S) - \gamma D_S} \frac{\cosh\left(\sqrt{\frac{\lambda+\gamma}{D_R}}(x_0+L)\right)\cosh\left(\sqrt{\frac{\lambda+\gamma}{D_R}}(x_0-L)\right)}{\sinh\left(2\sqrt{\frac{\lambda+\gamma}{D_R}}L\right)}$$

$$- \frac{\lambda+1+\frac{D_S\gamma}{\lambda(D_R-D_S)-\gamma D_S}}{\sqrt{\lambda D_S}} \frac{\cosh\left(\sqrt{\frac{\gamma}{D_S}}(x_0+L)\right)\cosh\left(\sqrt{\frac{\gamma}{D_S}}(x_0-L)\right)}{\sinh\left(2\sqrt{\frac{\gamma}{D_S}}L\right)}. \tag{30}$$

For the special case when $x_0 = 0$, this expression simplifies to

$$P(\lambda) = \frac{\gamma\sqrt{\frac{D_R}{\lambda+\gamma}}}{\lambda(D_R-D_S)-\gamma D_S} \frac{\coth\left(\sqrt{\frac{\lambda+\gamma}{D_R}}L\right)}{2} - \frac{\lambda+1+\frac{D_S\gamma}{\lambda(D_R-D_S)-\gamma D_S}}{\sqrt{\lambda D_S}} \frac{\coth\left(\sqrt{\frac{\gamma}{D_S}}L\right)}{2}. \tag{31}$$

In general, the NLEP problem (28) is difficult to tackle since P has such a complicated dependence on λ. However there are two cases for which stability of (28) is well established: namely, large or small $\frac{S_0^2}{\varepsilon}$. Note that S_0 is given by (17) and has two branches, S_{0+} and S_{0-}, refer to Figure 4. Consider the case of large N. Then $\frac{S_{0+}^2}{\varepsilon} \gg 1$ whereas $\frac{S_{0-}^2}{\varepsilon} \ll 1$. In the former case, (28) reduces to a *local* eigenvalue problem $(L_0 - \lambda)\psi \sim 0$. This problem is well known to admit a positive eigenvalue $\lambda = 5/4$ so that this branch is unstable. For the latter case ($S_0 = S_{0-}$), the problem (28) reduces to the following well-known NLEP problem:

$$\lambda\psi = L_0\psi - 2w^2 \frac{\int_{-\infty}^{\infty} w\psi dy}{\int_{-\infty}^{\infty} w^2 dy}, \quad S_0 \sim O(\varepsilon). \tag{32}$$

This is well-known to be *stable* as was first proven in [19].

Finally, a lengthy but a straightforward algebraic computation shows that at the fold point where $S_{0+} = S_{0-}$, there is a zero eigenvalue whose corresponding eigenfunction is given by $\psi = w$. This suggests that the entire branch S_{0+} is unstable whereas the entire branch S_{0-} is stable, although the proof of this fact is not in the cards due to the complex structure of $P(\lambda)$. This structure is analogous to the well-known properties of the Grey-Scott model in the low-feed regime [32].

Another approach is to consider the limit of large D_R and/or D_S (various so-called shadow limits). We do not observe any additional instabilities of a single spike in this regime so we will not pursue it further here.

4. SPIKE MOTION.

We now study the motion of the interior spike, which is determined by small eigenvalues. We rewrite the system as following:

$$\begin{cases} S_t = D_S S_{xx} - SI^2 + \gamma R, \\ I_t = \varepsilon^2 I_{xx} + SI^2 - I, \\ R_t = D_R R_{xx} + I - \gamma R \end{cases} \tag{33}$$

with Neumann boundary conditions and $D_S, D_R \gg O(\varepsilon^2)$. To study the motion of the spike, we expand around the center x_0 by writing $x = x_0 + \varepsilon y$, and let $x_0 = x_0(\varepsilon^2 t)$, $S(y,t) = S\left(\frac{x-x_0(\varepsilon^2 t)}{\varepsilon}\right)$, $I(y,t) = I\left(\frac{x-x_0(\varepsilon^2 t)}{\varepsilon}\right)$, and

$R(y,t) = R\left(\frac{x-x_0(\varepsilon^2 t)}{\varepsilon}\right)$. Then system (33) becomes

$$\begin{cases} -\varepsilon^3 x_0' S_y = D_S S_{yy} - \varepsilon^2 SI^2 + \varepsilon^2 \gamma R, \\ -\varepsilon x_0' I_y = I_{yy} + SI^2 - I, \\ -\varepsilon^3 x_0' R_y = D_R R_{yy} + \varepsilon^2 I - \varepsilon^2 \gamma R. \end{cases} \tag{34}$$

Applying the same expansion (6) and collecting ε order, we obtain that

$$\begin{cases} S_{1yy} = 0, \\ -x_0' I_{0y} = I_{1yy} + \chi S_1 I_0^2 + 2\chi S_0 I_0 I_1 - I_1, \\ R_{1yy} = 0, \end{cases} \tag{35}$$

in which S_0, I_0, R_0 are expressed in (17b), (12) and (13). Multipy the second equation by I_{0y} and integrate to obtain the solvability condition

$$x_0' \int_{-\infty}^{\infty} I_{0y}^2 dy = \frac{1}{3} \int_{-\infty}^{\infty} I_0^3 S_{1y} dy. \tag{36}$$

From (35), we know that S_1 is linear so that S_{1y} is a constant. To determine S_{1y}, we match to the outer region. We expand

$$\begin{aligned} S(x; x_0) &= S(x_0 + \varepsilon y; x_0) \\ &= S(x_0) + \varepsilon y S'(x_0), \end{aligned} \tag{37}$$

where $S(x; x_0)$ in outer region is expressed in (12). We then match it with the expansion (6) to have

$$S_1 = \left(-\frac{6\varepsilon}{S_0 D_S} G'(x_0; x_0)\right) y, \tag{38}$$

where $G(x; x_0)$ is expressed in (11). Therefore we have

$$S_{1y} = -\frac{6\varepsilon}{S_0 D_S} \begin{cases} G(x_0^+; x_0), & -L < x < x_0 \\ G(x_0^-; x_0), & x_0 < x < L. \end{cases} \tag{39}$$

Substituting (39) into the equation (36) gives the equation that describes the motion of the interior spike:

$$x_0' = -\frac{6\varepsilon}{D_S S_0^2} \frac{\sinh\left(2\sqrt{\frac{\gamma}{D_R}} x_0\right)}{\sinh\left(2\sqrt{\frac{\gamma}{D_R}} L\right)}, \tag{40}$$

where S_0 is expressed in (17b). Write

$$S_0 = \varepsilon \hat{S}, \tag{41}$$

then we have

$$\frac{dx_0}{dt} = -\frac{6\varepsilon}{D_S \hat{S}^2} \frac{\sinh\left(2\sqrt{\frac{\gamma}{D_R}} x_0\right)}{\sinh\left(2\sqrt{\frac{\gamma}{D_R}} L\right)}. \tag{42}$$

It's obvious to see that equation (42) has one equilibrium $x_0 = 0$, and the corresponding eigenvalue is

$$\lambda = -\frac{12\varepsilon}{D_S \hat{S}^2} \frac{\sqrt{\frac{\gamma}{D_R}}}{\sinh\left(2\sqrt{\frac{\gamma}{D_R}} L\right)} < 0. \tag{43}$$

Therefore the equilibrium centered at $x_0 = 0$ is stable with respect to spike motion.

4.1. Boundary effects and spike motion

From formula (43), it is clear that the eigenvalue is *stable*, provided that D_R is not too small. However numerical experiments show that the spike becomes unstable and moves to the boundary when D_R is of $O(\varepsilon^2)$. To understand this, note that for small D_R, (17b) simplifies to

$$S_0 \sim \frac{6\varepsilon(1 + \frac{1}{\gamma})}{N} \tag{44}$$

and $\hat{S} \sim \frac{6(1 + \frac{1}{\gamma})}{N}$. Therefore (43) simplifies to

$$\lambda \sim -\frac{2}{3}\frac{\varepsilon N^2}{D_S(1 + \frac{1}{\gamma})^2}\sqrt{\frac{\gamma}{D_R}}\exp\left(-2L\sqrt{\frac{\gamma}{D_R}}\right), \quad D_R \ll 1. \tag{45}$$

As such, the effect of $\langle S_x \rangle$ becomes exponentially small. On the other hand, there are also exponentially weak boundary effects due to the interaction of the pulse with the boundary that we disregarded in the computation leading to (36). These boundary terms appear when integrating by parts in (36). To compute them, we replace (36) by a more precise expression

$$-x_0'\int I_{0y}^2 dy = (I_{0y}I_{1y} - I_0 I_1)\big|_{y=-\frac{L-x_0}{\varepsilon}}^{y=\frac{L-x_0}{\varepsilon}} + \int I_{0y}I_0^2 S_1 dy. \tag{46}$$

The computation of the boundary terms is relatively standard and we summarize it here. Note that

$$w(y) \sim 6e^{-y} \text{ as } y \to \infty \tag{47}$$

so that

$$I_0 \sim \frac{6}{S_0}\exp(-y). \tag{48}$$

For x near L, we change variables:

$$x = L + \varepsilon z$$

so that $y = \frac{L-x_0}{\varepsilon} + z$ and

$$I_0 \sim \frac{6}{S_0}\exp\left(-\frac{L-x_0}{\varepsilon}\right)\exp(z). \tag{49}$$

Near $z = 0$, equation for I_1 satisfies $I_{1zz} - I_1 \sim 0$, so that $I_1 = A\exp z + B\exp(-z)$. Since $I'(L) = 0$, we must therefore have

$$I_1 \sim \frac{6\varepsilon}{S_0}\exp\left(-\frac{L-x_0}{\varepsilon}\right)\exp(-z), \tag{50}$$

so that

$$(I_{0x}I_{1x} - I_0 I_1)\big|_{x=L} = -\frac{72\varepsilon}{S_0^2}\exp\left(-2\frac{L-x_0}{\varepsilon}\right). \tag{51}$$

Performing a similar computation at $x = -L$, and evaluating the remaining terms as before, we obtain

$$x_0' \sim -\frac{6\varepsilon}{D_S}\frac{\sinh\left(2\sqrt{\frac{\gamma}{D_R}}x_0\right)}{\sinh\left(2\sqrt{\frac{\gamma}{D_R}}L\right)}\frac{1}{\hat{S}^2} + 60\varepsilon\left\{\exp\left(2\frac{x_0-L}{\varepsilon}\right) - \exp\left(2\frac{-L-x_0}{\varepsilon}\right)\right\} \tag{52}$$

so that

$$\lambda \sim -\frac{12\varepsilon}{D_S}\frac{\sqrt{\frac{\gamma}{D_R}}}{\sinh\left(2\sqrt{\frac{\gamma}{D_R}}L\right)}\frac{1}{\hat{S}^2} + 240\exp\left(-\frac{2L}{\varepsilon}\right). \tag{53}$$

This expression clearly shows that the boundary term can play a destabilizing effect when the first term on the right hand side of (53) is exponentially small. This happens precisely when D_R is small. Setting $\lambda = 0$, substituting $\hat{S} \sim \frac{6(1+\frac{1}{\gamma})}{N}$ and solving for D_s yields the critical value

$$D_S^* \sim \frac{\varepsilon N^2}{1440} \sqrt{\frac{\gamma}{D_R}} \exp\left(2L\left(\frac{1}{\varepsilon} - \sqrt{\frac{\gamma}{D_R}}\right)\right) \tag{54}$$

with a single spike centered at center being unstable when $D_S > D_S^*$, and stable otherwise. This phenomenon is illustrated in Figure 3. Take $L = 2, \gamma = 1, N = 5$ and $D_R = 0.005298$. Then (54) yields $D_S^* = 5.00$. It follows that a single spike is unstable at the origin when $D_R < 0.005298$ and is stable otherwise. This is confirmed in Figure 3.

The boundary effect discussed here is similar to destabilization discussed in [33]. However the difference here is that this effect is primarily driven by having a small D_R, and is very specific to having three components. Although the asymptotics of (54) are valid as long as $D_R \gg O(\varepsilon^2)$, similar destabilization phenomenon also happens when $D_R = O(\varepsilon^2)$. Although the asymptotics of (54) break down in such a case, numerics show that the destabilization phenomenon persists as D_S is increased.

5. INSTABILITY THRESHODLS OF MULTI-SPIKE EQUILIBRIUM

In this section we study K-spike patterns, where $K \geq 1$. We analyze two types of instabilities, one is referred to as spike competition or coarsening instability, whereby some of the spikes are annihilated if the initial state contains too many spikes. The other is referred to as self replication, whereby a new spike may appear by the process of spike splitting. In this chapter we derive explicit thresholds for these instabilities.

5.1. Coarsening

When there are too many spikes, some of them get absorbed by others. This is known as coarsening or competition instability. To determine the instability threshold for spike competition, we apply the method in [34, 35] and compute the critical value at which an asymmetric spike pattern bifurcates from symmetric branch. To do this, consider a single interior spike on the domain $[-l, l]$. Duplicating the domain K times we obtain K spikes on the domain of size $2L = 2lK$. From (13) we have:

$$S(l) = S_0 + \frac{3\varepsilon}{D_S S_0} \sqrt{\frac{D_R}{\gamma}} \left(\frac{1}{\tanh\left(\sqrt{\frac{\gamma}{D_R}}l\right)} - \frac{1}{\sinh\left(\sqrt{\frac{\gamma}{D_R}}l\right)}\right), \tag{55}$$

where $S_0 = S_{0-}$ is given in (17b) with $x_0 = 0$. Plots of $S(l)$ when $D_S = 1$ and $D_S = 3$ are shown in Fig 5. The bifurcation point corresponds to the minimum point of the curve $l \to S(l)$. Setting $S'(l) = 0$ then yields the critical stability threshold. Solving for D_S as a function of other parameters, and upon substituting $l = L/K$ we obtain the critical threshold

(a) $S(l)$ when $D_S = 1$

(b) $S(l)$ when $D_S = 3$
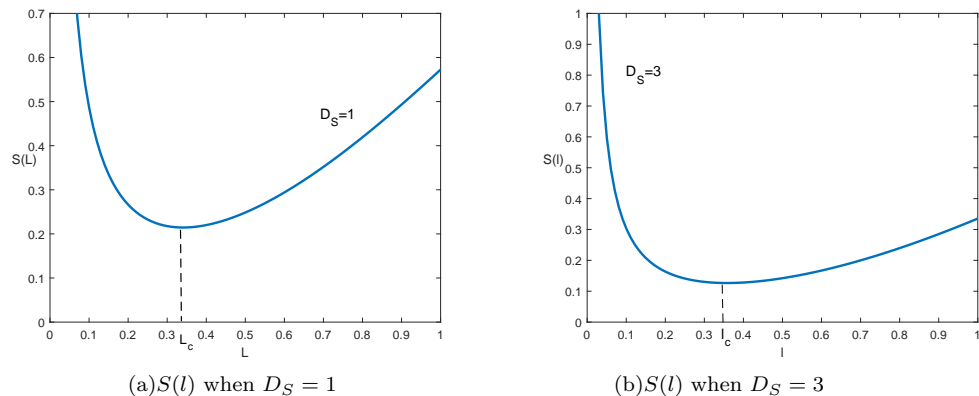
FIG. 5. Plots of function $S(l)$ versus l for $D_S = 1$ and $D_S = 3$. Other parameters are fixed and they are: $\varepsilon = 0.02, D_R = 2, \gamma = 1, N_0 = 4$.

$$D_{SK}^{com} \sim \frac{N_0^2 \left(\frac{L}{K}\right)^3}{3\varepsilon \left(1 + \frac{1}{\gamma}\right)^2} \left(1 - \frac{1}{\tanh^2\left(\sqrt{\frac{\gamma}{D_R}}\frac{L}{K}\right)} + \frac{\cosh\left(\sqrt{\frac{\gamma}{D_R}}\frac{L}{K}\right)}{\sinh^2\left(\sqrt{\frac{\gamma}{D_R}}\frac{L}{K}\right)}\right)$$
$$+ \frac{N_0^2 \left(\frac{L}{K}\right)^2}{3\varepsilon \left(1 + \frac{1}{\gamma}\right)^2} \sqrt{\frac{D_R}{\gamma}} \left(\frac{1}{\tanh\left(\sqrt{\frac{\gamma}{D_R}}\frac{L}{K}\right)} - \frac{1}{\sinh\left(\sqrt{\frac{\gamma}{D_R}}\frac{L}{K}\right)}\right). \tag{56}$$

The K-spike solution is unstable and some of the spikes will disappear when $D_S > D_{SK}^{com}$. The plot of D_{SK}^{com} as a function of D_R is shown in Figure 6. Note that D_{SK}^{com} has the following asymptotics as $D_R \to \infty$:

$$D_{SK}^{com} \sim \frac{N_0^2 \left(\frac{L}{K}\right)^3}{3\varepsilon \left(1 + \frac{1}{\gamma}\right)^2}, \quad \text{as } D_R \to \infty, \tag{57}$$

which is shown in Fig 6. We now summarize the following result:

Result 5.1 *Consider a K-spike solution for the system (3) on an interval of length $2L$ with $K > 1$. Then in the limit of $\varepsilon \to 0$, this solution is stable provided that $D_S < D_{SK}^{com}$, where D_{SK}^{com} is given by (56). When $D_S > D_{SK}^{com}$, the K-spike solution becomes unstable due to competition (or coarsening) instability and some of the spikes disappear.*
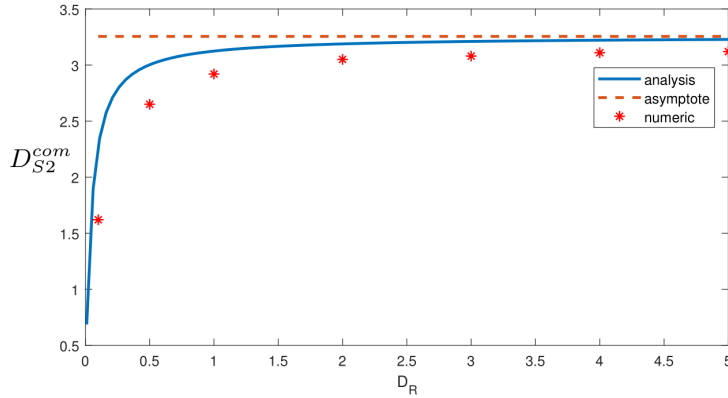
FIG. 6. Plot of stability threshold D_{S2}^{com} vs. D_R for single spike solutions. Here $\varepsilon = 0.02, L = 1, N_0 = 2.5$, and $\gamma = 1$. The curve denotes analysis value D_{S2}^{com} obtained by (56), and the dashed line is the asymptote of the curve. The dots are obtained by numeric simulations, and they have a good agreement with analysis.

5.2. Self-replication

Unlike coarsening instability, self-replication is related to disappearence of the single spike equilibrium solution. The mechanism has been studied in detail for Gray-Scott model [22, 23, 36–39], and it is similar here. We start by changing variables

$$S(x) = \frac{\varepsilon}{\sqrt{D_S}} \tilde{S}(x), I(x) = \frac{\sqrt{D_S}}{\varepsilon} \tilde{I}(x), x = \varepsilon y, \tag{58}$$

so that the system (3) transforms to

$$\begin{cases} \frac{\sqrt{D_S}}{\varepsilon} \tilde{S}_{yy} - \frac{\sqrt{D_S}}{\varepsilon} \tilde{S}\tilde{I}^2 + \gamma R = 0, \\ \tilde{I}_{yy} + \tilde{S}\tilde{I}^2 - \tilde{I} = 0, \\ \frac{D_R}{\varepsilon^2} R_{yy} + \frac{\sqrt{D_S}}{\varepsilon} \tilde{I} - \gamma R = 0. \end{cases} \tag{59}$$

Next, assume that D_S, D_R are $O(1)$. Then to leading order, in the inner region we obtain the following problem, referred to as the **core problem**,

$$\begin{cases} \tilde{S}_{yy} - \tilde{S}\tilde{I}^2 = 0, \\ \tilde{I}_{yy} + \tilde{S}\tilde{I}^2 - \tilde{I} = 0, \end{cases} \tag{60a}$$

this core problem is identical to the core problem for both the Grey-Scott model [22, 23, 36, 39], and the Schnakenberg model [27]. Assuming that the spike is symmetric, we define

$$A := \tilde{S}_y(\infty) = \int_0^\infty \tilde{S}\tilde{I}^2 dy. \tag{60b}$$

By plotting the numerical bifurcation diagram of (60b), it was found in [23, 39] that the steady state disappears when $A > A_c \approx 1.35$, and this disappearence leads to self-replication. To determine A in terms of the other parameters of the problem, we perform an asymptotic matching to the outer region. We estimate $\int SI^2 = \int I$ and

$$D_R R_{xx} - \gamma R = -\left(\int I dx\right)\delta(x), \quad D_S S_{xx} + \gamma R = -\left(\int I dx\right)\delta(x).$$

The solution is then given by

$$R(x) = \frac{(\int I dx)}{D_R} G(x), \tag{61a}$$

$$S(x) = -\frac{D_R}{D_S} R(x) + \frac{D_R}{D_S} R(0). \tag{61b}$$

where as before,

$$G(x) = \frac{\sqrt{\frac{D_R}{\gamma}}}{2\sinh\left(\sqrt{\frac{\gamma}{D_R}}l\right)} \begin{cases} \cosh\left(\sqrt{\frac{\gamma}{D_R}}(x+l)\right), & -l < x < 0 \\ \cosh\left(\sqrt{\frac{\gamma}{D_R}}(x-l)\right), & x < x < l. \end{cases} \tag{61c}$$

We substitute (61) into the total mass equation (14) to obtain that

$$N = 2N_0 l = 2A\sqrt{D_S}\left(1 + \frac{1}{\gamma} - \frac{D_R}{\gamma D_S}\right) + \frac{2Al}{\sqrt{D_S}}\frac{\sqrt{\frac{D_R}{\gamma}}}{\tanh\left(\frac{\gamma}{D_R}l\right)}, \tag{62}$$

so that self-replication occurs when

$$A = \frac{N_0 l\sqrt{D_S}}{D_S\left(1 + \frac{1}{\gamma}\right) + l\frac{\sqrt{\frac{D_R}{\gamma}}}{\tanh\left(\sqrt{\frac{\gamma}{D_R}}l\right)} - \frac{D_R}{\gamma}} > A_c \approx 1.35. \tag{63}$$

Equivalently, we rewrite (63) to obtain the following quadratic equation with respect to $\sqrt{D_S}$

$$\left(1 + \frac{1}{\gamma}\right)D_S - \frac{N_0 l}{A_c}\sqrt{D_S} + \frac{\sqrt{\frac{D_R}{\gamma}}l}{\tanh\left(\sqrt{\frac{\gamma}{D_R}}l\right)} - \frac{D_R}{\gamma} = 0. \tag{64}$$

Therefore replication of one-spike solution occurs when $D_S < D_S^{rep}$, where $\sqrt{D_S^{rep}}$ is the large root of (64). For K spikes on domain $[-L, L]$ with $L = Kl$, this leads to the following result:

Result 5.2 *Consider a K-spike solution of the system (3) on an interval of length $2L$ with $K \geq 1$. Then in the limit of $\varepsilon \to 0$, this solution is stable provided that $D_S > D_{SK}^{rep}$, where $D_S = D_{SK}^{rep}$ is the root of (64), in which $l = \frac{L}{K}$ and $A_c \approx 1.35$ corresponds to the fold point of the problem (60).*

Figure 7 shows numerical validation of Result 5.2. The solid curve denotes the asymptotic curve as given in Result 5.2. Above the curve, a single spike is stable. As D_S is decreased and crosses the curve, self-replication takes place resulting in two spikes. The dots denote numeric simulations. Good agreement is observed between numerics and asymptotics.

For a fixed D_R and a given number of spikes K, we have derived both upper and lower thresholds on the D_S for which K spikes are stable. Note that multiple solutions (e.g. two or three spikes) can be stable at the same time. This is illustrated in Figure 8.
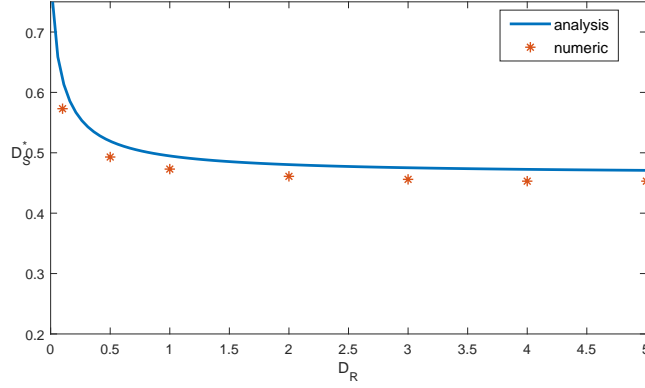
FIG. 7. Self-replication threshold (Result 5.2). Comparison between numerics and analysis. Solid curve is the analytical result given by (64). Dots denote numerical simulations. Self-replication is observed as D_S is decreased past the solid curve in the figure. Here $\varepsilon = 0.005, N = 5, L = 1$, and $\gamma = 1$.
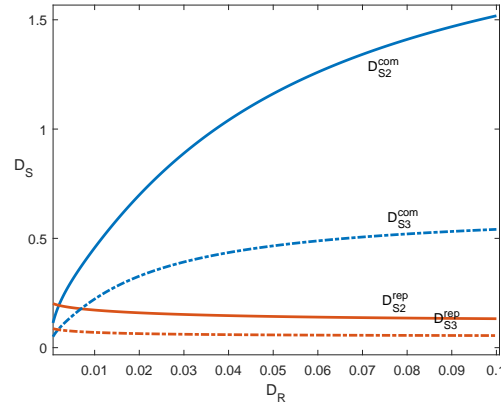
FIG. 8. Bifurcation diagram of K-spike patterns for $K = 2, 3$. The region between solid curves is the stable region for 2-spike patterns, and the region between dashed curves is the stable region for 3-spike patterns. Above the regions spike competition instability occurs, below the region, self replication instability occurs. Here $\varepsilon = 0.03, N_0 = 2.5, L = 1, \gamma = 1$.

6. MESA-LIKE STEADY STATES WHEN $D_R = 0$.

As shown in Section 5 5.1, multi-spike configurations lose stability when D_R is sufficiently small: even a single spike eventually becomes unstable (due to an exponentially small eigenvalue becoming positive) and moves towards the boundary when $D_R = O(\varepsilon^2)$. For even smaller values of D_R, we observe numerically that the spike "fattens" as shown in Figure 9. In the limit of $D_R \to 0$, numerics indicate a phase separation of infected population. This can be thought of as a "quaranteene effect": when mobility of recovered population and susceptible population is reduced, the infected population is confined to a certain region of the entire domain with a sharp interface inbetween.

Here we perform the analysis for the limiting case $D_R = 0$ and D_S being small, although similar results hold even when $D_R = D_S$ and is nonzero. At the steady steate, we then have $I = \gamma R$ so that the model (3) reduces to

$$\begin{cases} 0 = D_S S_{xx} - SI^2 + I, \\ 0 = \varepsilon^2 I_{xx} + SI^2 - I. \end{cases} \tag{65}$$

Adding the two equations we we obtain that $D_S S + \varepsilon^2 I$ is constant. We then eliminate S from the second equation to obtain

$$D_S I_{xx} = \frac{D_S}{\varepsilon^2} I - CI^2 + I^3, \tag{66}$$

where

$$C = I + \frac{D_S}{\varepsilon^2} S \tag{67}$$
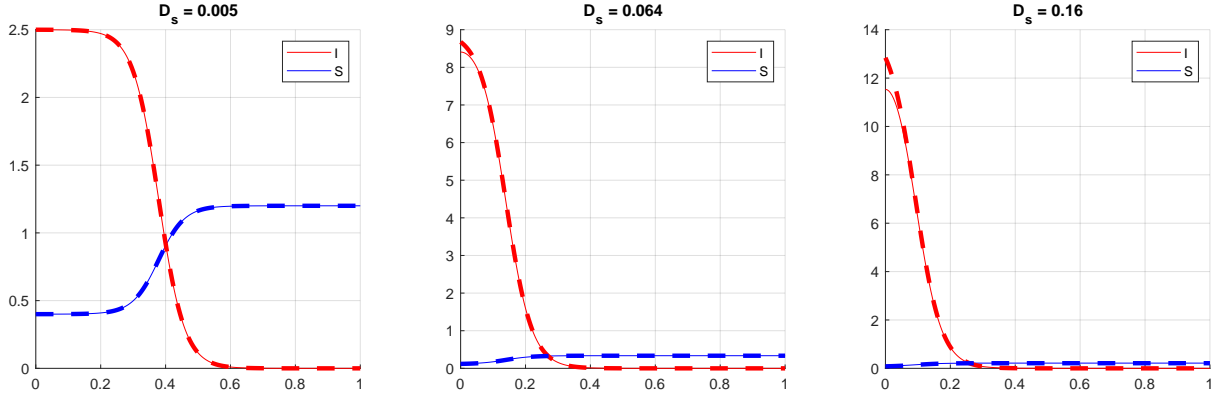
FIG. 9. Steady states of the system (3) with $L = 1, D_R = 0, \varepsilon = 0.04, \gamma = 1, N_0 = 2.79$ and with D_S as indicated. Solid curves correspond to the full numerical solution of (3). Dashed lines show the asymptotic approximation (69).

is a constant to be determined.

Equation (66) admits a heteroclinic solution connecting the steady state $I = 0$ to a positive steady state I_+ provided that the Maxwell-line condition holds: $\int_{I0}^{I_+} \left(\frac{D_S}{\varepsilon^2}I - CI^2 + I^3\right) dI = 0$. This is equivalent to cubic having equidistant roots, that is,

$$\frac{D_S}{\varepsilon^2}I - CI^2 + I^3 = I\left(I - \frac{I_+}{2}\right)(I - I_+) \tag{68}$$

so that

$$I_+ = \sqrt{\frac{2D_S}{\varepsilon^2}}, \quad C = \frac{3}{2}I_+. \tag{69a}$$

In this case there is an interface solution on the domain $[0, L]$ given by

$$\gamma R = I \sim I_+ \left(\frac{1}{2}\tanh\left(\frac{I_+}{2\sqrt{2}}\frac{(l - |x|)}{\sqrt{D_S}}\right) + \frac{1}{2}\right); \tag{69b}$$

$$S \sim \frac{\varepsilon^2}{D_S}I_+ \left(1 - \frac{1}{2}\tanh\left(\frac{I_+}{2\sqrt{2}}\frac{(l - |x|)}{\sqrt{D_S}}\right)\right). \tag{69c}$$

Here, l is the location of the interface. A back-to-back interface solution such as shown in figure 3 is obtained by extending this solution to $[-L, L]$ using even reflection. Finally, the interface location l is determined using the mass conservation condition, $N_0 L = \int_0^L (S + I + R)dx$. In the limit $\varepsilon \to 0$, this yields

$$LN_0 = I_+ \left\{\left(1 + \frac{1}{\gamma}\right)l + \left(\frac{3}{2}L - \frac{1}{2}l\right)\left(\frac{\varepsilon^2}{D}\right)\right\}$$

so that solving for l we obtain

$$l = \frac{N_0 - I_+ \frac{3}{2}\left(\frac{\varepsilon^2}{D}\right)}{I_+ \left(1 + \frac{1}{\gamma} - \left(\frac{\varepsilon^2}{D}\right)\right)}L. \tag{69d}$$

This result is valid as long as $O(\varepsilon) \ll l < L$. In this case, the interface has an exponentially weak effect on the boundary, and the agreement with the numerics is nearly perfect. Figure illustrates this. Solution (69) is shown super-imposed on the numerical solution; the difference is imperceptible in the "eye-ball norm" as long as $l = O(1)$. The asymptotics break down when l becomes small (figure 9, right), and the interface transforms into a spike solution.

Note that the infected class subdivides the domain into outbreak portion ($x < l$) and disease-free portion ($x > l$). The susceptible population is three times smaller within the outbreak portion of the domain when compared with the disease-free portion.

For simplicity, we took $D_R = 0$ here. Numerical simulations indicate that similar interface solutions persist for sufficiently small D_R, although it changes l as well as the interface shape. We defer their study to future work.
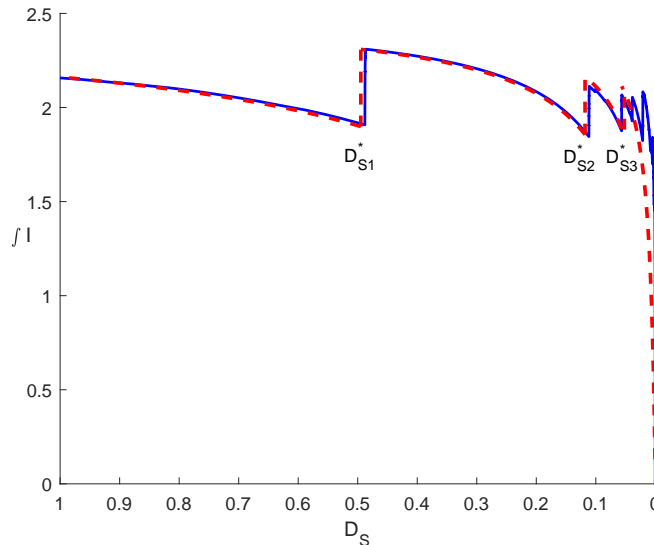
FIG. 10. Total mass of infected people versus D_S. Here $\varepsilon = 0.005, N = 5, D_R = 1, L = 1$, and $\gamma = 1$. The solid curve denotes numeric results, and dashed curves is the asymptotic result corresponding to self-replication thresholds of Result 5.2.

7.   DISCUSSION

In this paper we studied the consequence of adding spatial diffusion to the relatively-standard SIRS model. Under certain reasonable assumptions, the resulting system (3) has a very rich solution space, exhibiting hot-spots as well as interface-type solutions, depending on whether D_R is large or small, respectively.

Occurrence of disease clusters has been widely documented in epidemiology literature, see e.g. [5–7, 40, 41]. Our study underscores the importance of diffusion in formation of hot-spots and disease spread. One of the key assumptions leading to hot-spot formation was that the diffusion of infected class is relatively slow compared to the susceptible class. While it is difficult to measure (or even quantify) diffusion rates, one study [7] did find a strong positive correlation between HIV hot-spot location and proximity to a large road. A multitutde of other causes have been proposed (see [40] and references therein). This includes the level of male circomcision; religiosity (less HIV prevalence in muslum communities in Africa); urbanization level with wider HIV prevalence in rural areas, among others; preponderence of drug use [41].

The hot-spot regime $D_R \gg D_I$ is very similar to the previous analysis for the two-component reaction-diffusion systems, such as the Schnakenberg model [27, 35], and the behaviour is qualitatively similar to the SI model with diffusion introduced in [16] (which itself is a generalization of the Schnakenberg model). However, from the analysis point of view, the third component introduces a novel non-local eigenvalue problem (see Section 3). On the other hand, the regime $D_R \leq D_I$ requires completely new analysis. On one hand, the resolution of an exponentially small boundary layer in Section 4 4.1 is crucial for computing stability thresholds of a single interior spike in this regime. On the other, this regime also leads to mesa-type solutions of Section 6. The analysis there is similar to interface solutions derived in [42, 43] for the Gray-Scott model. However it appears to be more robust: such interface solutions exist for a wide range of parameters here, rather than a very narrow range studied in [42, 43].

In Figure 10 we plot the total mass of infected population versus D_S. As D_S is decreased, the mobility of susceptible population is reduced and initially leads to a decrease of overall disease load. However as D_S is decreased further, eventually a self-replication threshold is triggered. This results in an immediate increase of infection hot-spots and an overall increase in infected population. This underscores a highly nonlinear relationship between mobility and disease outbreaks.

[1] William Ogilvy Kermack and Anderson G McKendrick. A contribution to the mathematical theory of epidemics. *Proceedings of the royal society of london. Series A, Containing papers of a mathematical and physical character*, 115(772):700–721, 1927.

[2] Zhilan Feng and Jorge X Velasco-Hernández. Competitive exclusion in a vector-host model for the dengue fever. *Journal of mathematical biology*, 35(5):523–544, 1997.

[3] Herbert W Hethcote. The mathematics of infectious diseases. *SIAM review*, 42(4):599–653, 2000.

[4] P van den Driessche. A simple sis epidemic model with a backward bifurcation p. van den driessche*, james watmough** department of mathematics and statistics, university of victoria, victoria, bc v8w 3p4, e-mail: pvdd@ math. uvic. ca, watmough@ math. uvic. ca april 26, 2000. 2000.

[5] Leo C Zulu, Ezekiel Kalipeni, and Eliza Johannes. Analyzing spatial clustering and the spatiotemporal nature and trends of hiv/aids prevalence using gis: the case of malawi, 1994-2010. *BMC infectious diseases*, 14(1):285, 2014.

[6] Phaisarn Jeefoo. Spatial patterns analysis and hotspots of hiv/aids in phayao province, thailand. *Archives Des Sciences*, 65(9):37–50, 2012.

[7] Frank Tanser, Till Bärnighausen, Graham S Cooke, and Marie-Louise Newell. Localized spatial clustering of hiv infections in a widely disseminated rural south african epidemic. *International journal of epidemiology*, 38(4):1008–1016, 2009.

[8] Henryk Fuks and Anna T Lawniczak. Individual-based lattice model for spatial spread of epidemics. *Discrete Dynamics in Nature and Society*, 6(3):191–200, 2001.

[9] Ruth J Doran and Shawn W Laffan. Simulating the spatial dynamics of foot and mouth disease outbreaks in feral pigs and livestock in queensland, australia, using a susceptible-infected-recovered cellular automata model. *Preventive veterinary medicine*, 70(1-2):133–152, 2005.

[10] Julien Arino and P Van den Driessche. A multi-city epidemic model. *Mathematical Population Studies*, 10(3):175–193, 2003.

[11] Alun L Lloyd and Vincent AA Jansen. Spatiotemporal dynamics of epidemics: synchrony in metapopulation models. *Mathematical biosciences*, 188(1-2):1–16, 2004.

[12] Julien Arino, Richard Jordan, and P Van den Driessche. Quarantine in a multi-species epidemic model with spatial dynamics. *Mathematical biosciences*, 206(1):46–60, 2007.

[13] Hua Yuan and Guoqing Chen. Network virus-epidemic model with the point-to-group information propagation. *Applied Mathematics and Computation*, 206(1):357–367, 2008.

[14] Marcelo Kuperman and Guillermo Abramson. Small world effect in an epidemiological model. *Physical Review Letters*, 86(13):2909, 2001.

[15] James D Murray. *Mathematical biology. II Spatial models and biomedical applications {Interdisciplinary Applied Mathematics V. 18}*. Springer-Verlag New York Incorporated New York, 2001.

[16] Gui-Quan Sun. Pattern formation of an epidemic model with diffusion. *Nonlinear Dynamics*, 69(3):1097–1104, 2012.

[17] Let $t = \frac{\hat{t}}{\nu}, S = \sqrt{\frac{\nu}{\chi}}\hat{S}, I = \sqrt{\frac{\nu}{\chi}}\hat{I}, R = \sqrt{\frac{\nu}{\chi}}\hat{R}$ and define new parameters by $\gamma = \nu\hat{\gamma}, D_S = \nu\hat{D_S}, D_I = \nu\varepsilon^2, D_R = \nu\hat{D_R}$. Upon dropping the hats, this yields (3).

[18] Juncheng Wei and Matthias Winter. *Mathematical aspects of pattern formation in biological systems*. Springer, 2013.

[19] Juncheng Wei. On single interior spike solutions of the gierer–meinhardt system: uniqueness and spectrum estimates. *European Journal of Applied Mathematics*, 10(4):353–378, 1999.

[20] David Iron, Michael J Ward, and Juncheng Wei. The stability of spike solutions to the one-dimensional gierer–meinhardt model. *Physica D: Nonlinear Phenomena*, 150(1):25–62, 2001.

[21] David Iron and Michael J Ward. The dynamics of multispike solutions to the one-dimensional gierer–meinhardt model. *SIAM Journal on Applied Mathematics*, 62(6):1924–1951, 2002.

[22] Cyrill B Muratov and VV Osipov. Stability of the static spike autosolitons in the gray–scott model. *SIAM Journal on Applied Mathematics*, 62(5):1463–1487, 2002.

[23] CB Muratov and Vyacheslav V Osipov. Static spike autosolitons in the gray-scott model. *Journal of Physics A: Mathematical and General*, 33(48):8893, 2000.

[24] A Doelman, RA Gardner, and TJ Kaper. Large stable pulse solutions in reaction-diffusion equations. *Indiana University Mathematics Journal*, 50(1):443–507, 2001.

[25] Theodore Kolokolnikov, Michael J Ward, and Juncheng Wei. The existence and stability of spike equilibria in the one-dimensional gray–scott model on a finite domain. *Applied mathematics letters*, 18(8):951–956, 2005.

[26] K Kang, T KOLOKOLNIKOV, and MJ Ward. The stability and dynamics of a spike in the one-dimensional keller-segel model. *IMA J. Appl. Math*, 2005.

[27] Theodore Kolokolnikov and Juncheng Wei. Pattern formation in a reaction-diffusion system with space-dependent feed rate. *SIAM Review*, 60(3):626–645, 2018.

[28] Jonathan A Sherratt and Gabriel J Lord. Nonlinear dynamics and pattern bifurcations in a model for vegetation stripes in semi-arid environments. *Theoretical population biology*, 71(1):1–11, 2007.

[29] K.J. Painter and T. Hillen. Spatio-temporal chaos in a chemotaxis model. *Physica D: Nonlinear Phenomena*, 240(4):363–375, 2011.

[30] Philip K Maini, Thomas E Woolley, Ruth E Baker, Eamonn A Gaffney, and S Seirin Lee. Turing's model for biological pattern formation and the robustness problem. *Interface focus*, page rsfs20110113, 2012.

[31] Andreas Buttenschoen, Theodore Kolokolnikov, Michael J Ward, and Juncheng Wei. Cops-on-the-dots: The linear stability of crime hotspots for a 1-d reaction-diffusion model of urban crime. 2018.

[32] Theodore Kolokolnikov, Michael J Ward, and Juncheng Wei. The existence and stability of spike equilibria in the one-dimensional gray–scott model: The low feed-rate regime. *Studies in Applied Mathematics*, 115(1):21–71, 2005.

[33] Theodore Kolokolnikov and Michael J Ward. Bifurcation of spike equilibria in the near-shadow gierer-meinhardt model. *DSDS B*, 4:1033–1064, 2004.

[34] Theodore Kolokolnikov, Michael Ward, and Juncheng Wei. The stability of steady-state hot-spot patterns for a reaction-diffusion model of urban crime. *arXiv preprint arXiv:1201.3090*, 2012.

[35] Michael J Ward and Juncheng Wei. The existence and stability of asymmetric spike patterns for the schnakenberg model.

Studies in Applied Mathematics, 109(3):229–264, 2002.

[36] William N Reynolds, John E Pearson, and Silvina Ponce-Dawson. Dynamics of self-replicating patterns in reaction diffusion systems. *Physical review letters*, 72(17):2797, 1994.

[37] William N Reynolds, Silvina Ponce-Dawson, and John E Pearson. Self-replicating spots in reaction-diffusion systems. *Physical Review E*, 56(1):185, 1997.

[38] Arjen Doelman, Tasso J Kaper, and Paul A Zegeling. Pattern formation in the one-dimensional gray-scott model. *Nonlinearity*, 10(2):523, 1997.

[39] Theodore Kolokolnikov, Michael J Ward, and Juncheng Wei. The existence and stability of spike equilibria in the one-dimensional gray–scott model: the pulse-splitting regime. *Physica D: Nonlinear Phenomena*, 202(3-4):258–293, 2005.

[40] Lucy Andere Otwombe. *Spatial distribution and analysis of factors associated wiyh HIV infection among young people in Eastern Africa: applied to the MEASURE demographic and health survey data collected between 2007 and 2011*. PhD thesis, 2014.

[41] Gina Rae Kruse, Russell Barbour, Robert Heimer, Alla V Shaboltas, Olga V Toussova, Irving F Hoffman, and Andrei P Kozlov. Drug choice, spatial distribution, hiv risk, and hiv prevalence among injection drug users in st. petersburg, russia. *Harm reduction journal*, 6(1):22, 2009.

[42] JK Hale, Lambertus A Peletier, and William C Troy. Stability and instability in the gray-scott model: the case of equal diffusivities. *Applied mathematics letters*, 12(4):59–65, 1999.

[43] JK Hale, LA Peletier, and William C Troy. Exact homoclinic and heteroclinic solutions of the gray–scott model for autocatalysis. *SIAM Journal on Applied Mathematics*, 61(1):102–130, 2000.